

STUDY ON DISLOCATION CELL STRUCTURE, DISLOCATION DENSITY-FATIGUE PROPERTY RELATIONSHIP OF A STRUCTURAL STEEL

Nguyen Ngoc Vinh^{a,*}

^a*Department of Infrastructure Engineering, Vietnam Japan University,
Luu Huu Phuoc street, Nam Tu Liem district, Hanoi, Vietnam*

Article history:

Received 24/5/2021, Revised 14/01/2022, Accepted 17/01/2022

Abstract

In this study, the evolution of the dislocation cell structure and variation of mechanical properties of structural steel under low-cycle fatigue were studied using the indentation experiment, optical microscope, and transmission electron microscope examinations. The results indicated that the dislocation cell structure was well-formed under cyclic loading. When the strain amplitude increased, the original grains were broken more, leading to the dislocation cell size tended to decrease, while dislocation density showed an increase with the further increase of strain amplitude from 0.4% to 1.0%, respectively. Both indentation hardness and yield stress tend to increase when the cyclic loading increases. The change in the dislocation structure was responsible for the strengthening of fatigue mechanical properties, meaning that the dislocation density tended to increase, while the dislocation cell size showed a decrease with the further increase of fatigue condition, leading to the increase of both hardness and yield strength since mechanical properties were inversely proportional to the mean cell size. The results of this study can be used for the practical designs as well as to understand the microstructure changes in structural steel subjected to cyclic loading.

Keywords: cyclic loading; dislocation cell; dislocation density; grain boundary strengthening; microstructure; indentation.

[https://doi.org/10.31814/stce.huce\(nuce\)2022-16\(1\)-03](https://doi.org/10.31814/stce.huce(nuce)2022-16(1)-03) © 2022 Hanoi University of Civil Engineering (HUCE)

1. Introduction

Structural steel has been extensively employed in buildings, bridges, tunnels, automobiles, frames, oil rigs, and machinery parts due to its favorable material properties, i.e. high strength, toughness, ductility, and stiffness [1–4]. During the fabrication process, it is rolled, cut, and turned into many shapes without the change of physical properties and composition due to its excellent ductility [5]. Since structural steel has high durability, ductility, and energy dissipation capacity [6], the steel structures have a great ability to withstand dynamic and seismic loadings. Thus, this type of steel is more suitable for both static and dynamic applications and is attributed a suitable material to construct buildings, bridges, tunnels, and so on. The mechanical properties of structural steel strongly depend on both service conditions and metallurgy factors, including temperature, environmental conditions, and especially the state of loading histories [7–9]. Ye et al. [10] pointed out that the degradation of

*Corresponding author. *E-mail address:* nn.vinh@vju.ac.vn (Vinh, N. N.)

mechanical properties can be easily observed during the service time under the impacts of operating under alternating or dynamic loading conditions. The deterioration of mechanical properties of steel components caused by the dynamic and seismic loadings was called fatigue damage [11]. These loadings influence not only local mechanical properties but also the microstructure or the dislocation structure of the damaged specimens. Therefore, there is a lot of attention on the fatigue behavior of several types of steel as well as the evolution of microstructure [9, 12–18].

Srinivasan et al. [12] characterized the influences of the temperature on the low-cycle fatigue behavior of 316L stainless steel, indicating that the fatigue life of 316L stainless steel strongly depended on temperature and reached a maximum value at a temperature of around 573 K. At elevated temperatures, the fatigue life tended to drastically decrease with the further increase of the temperature. Furthermore, the authors also pointed out that low-cycle fatigue experiment introduced some amount of planar slip at all temperatures and the presence of well-defined slip bands with piling up dislocations could be observed more frequently at 873 K. Ye et al. [13] investigated multi-scale deformation of 18Cr-8Ni austenitic steel under cyclic loading, pointing out that when the strain amplitude increased, the formation of dislocation cell of the specimens deformed by cyclic loading can be observed and the dislocation cell size tended to progressively decrease. Generally, the microstructural evolution of the specimen deformed by low-cycle fatigue strongly depends on the amplitude of applied strain, being responsible for the variation of the local deformation resistance of cyclically deformed specimens at various scales. The influences of cyclic loading on semi-static mechanical properties of the material, fracture behavior, and the evolution of microstructure of 304 stainless steel were then conducted by Ye et al. [9]. The research showed the increase of slip band density within the grains and the number of grains with the further increase of straining cycles as well as the increase of deformation amount induced austenite/martensite transformation.

Veerababu et al. [14] presented the fatigue behavior of grade 92 steel weld joints, showing that welded specimens were found to have similar fatigue life compared with those of the base metal specimen at a higher amplitude of applied strain. At lower amplitude of applied strain, the welded specimens have a lower fatigue life than those in the base metal specimen and the failures were usually observed at the base metal region for all levels of strain amplitudes from $\pm 0.4\%$ to $\pm 1.0\%$. Tsai et al. [15] then characterized the fatigue behavior and microstructure of a duplex stainless steel weld metal under vibration-assisted welding. The microstructure of SAF 2507 weld metals consisted of δ -ferrite, Widmanstätten (W), intragranular (IG), and allotriomorphic austenite, and the fatigue behaviors in all deformed samples exhibited the initial hardening followed by gradual softening. Also, Nguyen et al. [16] have investigated the variation of mechanical properties of SS400 structural steel under low-cycle fatigue, while microstructure of fatigue-tested F82H steel under multi-axial loadings was recently studied by Fukumoto et al. [17]. The research exhibited that for all fatigue loading conditions, dislocation density tended to increase at 50 cycles; however, for multi-axial loading, this dislocation density varied only modestly during the fatigue deformation process. Low-cycle fatigue properties, damage mechanism, life prediction, and microstructure of MarBN steel were also conducted by Zhang et al. [18]. Although the relationship between cyclic softening and microstructure at different temperatures was discussed; however, the correlation of microstructural evolution to the variation of mechanical properties has not yet been investigated. Thus, it is necessary to have a comprehensive study to investigate the microstructural change as well as the degradation of mechanical properties subjected to cyclic loading.

In this study, the development of the dislocation cell structure and variation of mechanical properties of structural steel subjected to cyclic loading was investigated using the indentation experiment,

optical microscope, and transmission electron microscope examinations. Furthermore, the influences of strain amplitude on the characteristics of deformed microstructure under cyclic loading, for example, dislocation density, dislocation cell size, as well as the relationship between the variation of mechanical properties and fatigue levels were studied. Finally, the new model for structural steel was also established to describe the relationship between the low-cycle fatigue and the characteristics of microstructure under cyclic loading.

2. Methodology

2.1. Estimation of material properties from indentation curve

The methodology to determine the mechanical properties of the material has been presented in several previous works [19–21]. However, the description of the method to extract mechanical properties from the characteristics of the load-displacement curve (see Fig. 1) was briefly presented as follows. Oliver and Pharr [22, 23] established a famous and general method to evaluate the mechanical properties of the material from the loading/holding/unloading curves. Therefore, elastic modulus (E) and hardness (H) can be easily calculated using Eq. (1) and Eq. (2), respectively.

$$H = \frac{P_m}{A_c} \tag{1}$$

$$E = (1 - \nu^2) \left[\frac{1}{E_r} - \frac{1 - \nu_i^2}{E_i} \right]^{-1} \tag{2}$$

$$E_r = \frac{\sqrt{\pi} S}{2\beta \sqrt{A_c}} \tag{3}$$

The contact area is denoted as A_c , while E_r is as the reduced modulus, determined based on the values of the stiffness of the contact (S) and the contact depth (h_c) as described in Eq. (3). The notation β in Eq. (3) is a constant factor depending on the shape of the indenter tip [24]. In Fig. 1, W_t , W_e , W_p , h_m , and h_r are the total work, elastic work, plastic work, maximum displacement, and final displacement, respectively.

For plastic properties, i.e. yield stress, strain hardening exponent, and plastic property α , it needs to have the help of dimensional analysis as well as the reverse algorithm to construct the basic relationship between the constitutive parameters and the characteristics of the indentation curve. Many researchers [23, 25–27] proposed the methodology to estimate the plastic properties of the material, for example, Dao’ method for elasto-plastic steels [28], Pham & Kim’s method [23], and Nguyen et al. [29] for structural steel of which stress-strain curve includes elastic, plastic plateau, and hardening parts [1]. The main objective of this study is to investigate the dislocation cell structure of structural steel under low-cycle fatigue, the distribution of the dislocation cell size, as well as its contribution to the variation of mechanical

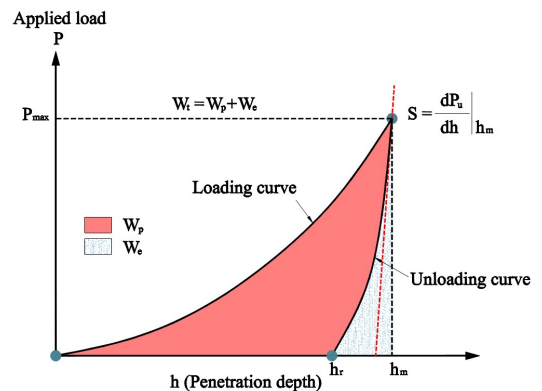


Figure 1. Indentation responses from depth-sensing indentation experiment showing the loading/unloading stage

properties of structural steel. Thus, Pham & Kim's method was applied to determine yield stress and strain hardening exponent of SS400 structural steel in this study, and this method was described as shown in two main dimensionless functions as

$$\frac{E_r^*}{\sigma_y} = \Pi_1 = \sum_{i=1}^4 \sum_{j=1}^4 \sum_{k=1}^3 \left[a_{ijk} n^{j-i} \alpha^{k-1} \left(\frac{E_r}{C} \right)^{i-1} \right] \quad (4)$$

$$\frac{S}{E_r^* h_m} = \Pi_2 = \sum_{i=1}^4 \sum_{j=1}^4 \sum_{k=1}^3 \left[b_{ijk} n^{j-i} \alpha^{k-1} \ln \left(\frac{E_r}{\sigma_y} \right)^{i-1} \right] \quad (5)$$

In Eqs. (4) and (5), a_{ijk} and b_{ijk} are the dimensional coefficients and C is the loading curvature of the loading curve.

2.2. Estimation of the dislocation density

Under the fatigue conditions, the dislocation structure was formed depending on the strain amplitude levels. Furthermore, one of the characteristics of dislocation structure is dislocation density (ρ). Thus, the determination of dislocation density is quite important. First, the formation of the dislocation structure of the specimens deformed by cyclic loading can be observed using the transmission electron microscope (TEM) and optical microscope (OM) examinations. ρ and the dislocation cell size (d) are then calculated based on the microimages and their sketch of the dislocation structure. Regarding ρ , there are two different methods to determine the dislocation density, such as X-ray and TEM. To reduce the complexity of the research, the dislocation density of the samples deformed by cyclic loading is determined from the TEM image using the following equation

$$\rho = \frac{N_{\text{Intersection}}}{A} \quad (6)$$

in which A and $N_{\text{Intersection}}$ are a tested area and the number of intersections of the dislocation lines and the surface plan. Both values of $N_{\text{Intersection}}$ and A are obtained from the TEM images. For the dislocation cell size, the distribution of cell size will be calculated first, and then the average values of dislocation cell size can be determined based on a histogram of the statistic of dislocation cell size distribution.

3. Experimental procedures

The material for this study is SS400 structural steel with the chemical composition of 0.05C, 0.037%Si, 0.46%Mn, 0.013%P, 0.002%S, 0.011%Al, 0.0017%Ca, and Fe balance. The method for the preparation of indentation specimens as well as the indentation process can be found out elsewhere [19, 30]. It should be noted that the preparation of indentation specimens must comply with the ASTM standard [31] and the indentation process also follows the ISO 14577 standard [32]. The polished specimens are recommended to conduct the indentation process as soon as possible after polishing the flat sample surface to minimize the oxidation of the specimen surface [33]. The Nano-Hardness tester was shown in Fig. 2. In this study, Berkovich indenter tip was employed to conduct all indentation experiments.

There are few methods to exam the topography of samples, such as optical microscope (OM), scanning electron microscope (SEM), and transmission electron microscopy (TEM) examinations.

These methods are usually used to investigate the sample surface, depending on the using scales, for example, micrometer (the OM examination), tens nanometers (the SEM examination), and few nanometers (the TEM examination). Since the main purpose of this study is to investigate the dislocation cell structure of structural steel under cyclic loading, the TEM examination was adopted to obtain the micro-image of microstructures. First, three thin slices were cut out from the cross-section in the middle part near the fracture location of the deformed low-cycle specimens. These thin slices were then electro-polished with the precision ion polishing system (PIPS) technique. Finally, the TEM examinations were conducted on these polished specimens using the TEM HF-3300 machine as seen in Fig. 3.

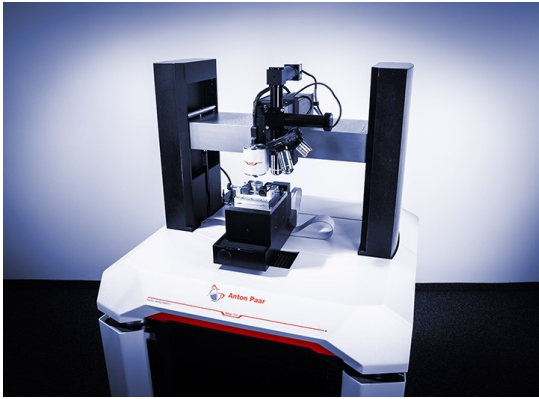


Figure 2. Depth-Sensing indenter tip for indentation testing



Figure 3. HF-3300 machine for the TEM examination

4. Results and discussion

4.1. Dislocation structure under low-cycle fatigue

Under cyclic loading, the dislocation lines were developed and well-observed using the TEM examination. In this study, the dislocation structure of the virgin sample was presented for comparison purposes as seen in Fig. 4. It can be recognized that the initial microstructure contains the straight dislocation lines with a low density of dislocation as a result of the fabrication of steel plate. These dislocation lines distribute randomly and unevenly on the Ferrite regions. The thickness of the dislocation line is so thin, leading to the difficulty to observe the dislocation line distribution.

With the presence of cyclic loading, the dislocation cell structure was partially formed as seen in Fig. 5 for the case of low strain amplitude. As seen, the shape of the dislocation cell is quite clear in several regions; however, it is quite difficult to distinguish the dislocation cell boundaries. Another interesting feature of Fig. 5 is the appearance of packets of the dislocation debris under cyclic loading (strain amplitude of 0.4%). The initial grains are forced to be broken under the applied stress range corresponding to the strain amplitude. However, this applied stress is not strong enough due to a low strain amplitude, leading to the partial formation of dislocation cell structure and the packets of dislocation debris. These packets of dislocation debris can be observed to be located inside the original grains and the dislocation debris boundaries are not pronounced for this low level of cyclic loading. When the number of cycles increases during the fatigue process, the dislocation lines can be developed inside the dislocation cells and the boundaries of the dislocation cell. However, the dislocation density

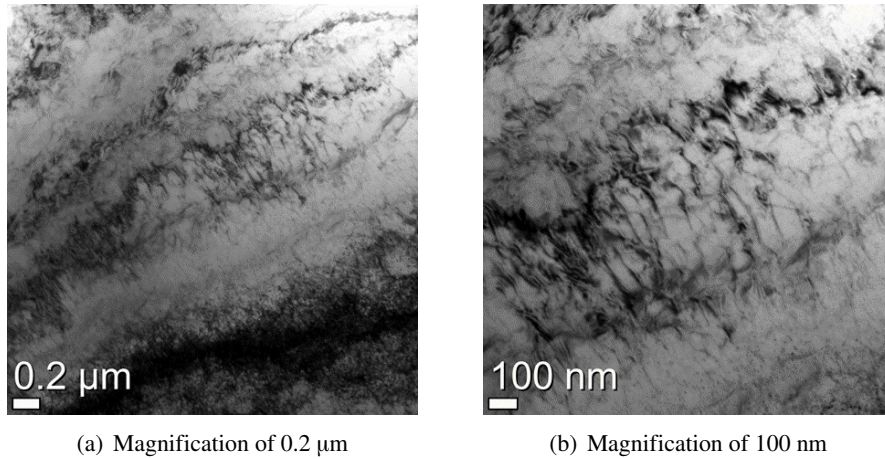


Figure 4. Dislocation structure of virgin specimen showing the dislocation lines with a low density of dislocation

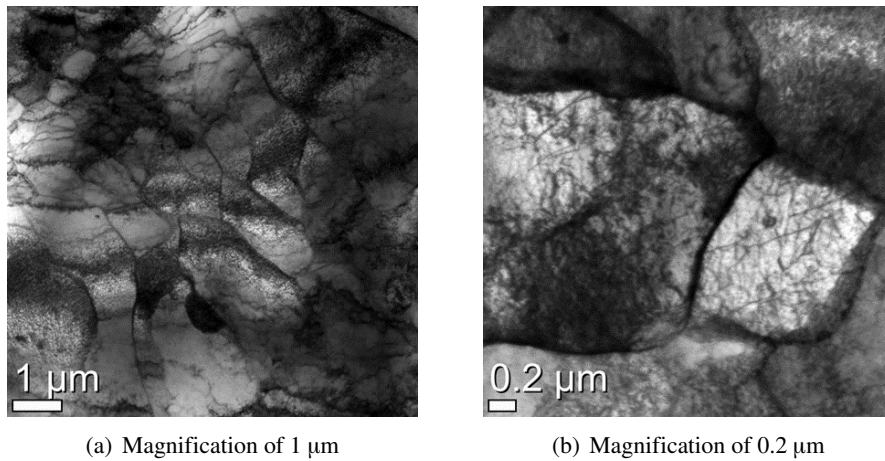


Figure 5. Dislocation structure of the specimens deformed by cyclic loading at $\varepsilon_a = 0.4\%$

is unevenly distributed. When the applied strain amplitude increases, the formation of dislocation cell size is more pronounced as observed in Fig. 6. The size of dislocation cells is relatively smaller than those at the lower strain amplitude level. This might be caused by the increase in the applied stress range, resulting in the original grains being broken more and the smaller dislocation cells can be observed more frequently. Moreover, the dislocation lines are fully developed inside the dislocation cells, leading to the relative increase of dislocation density as seen in Fig. 6. At highest the strain amplitude level, the dislocation lines are fully developed inside all dislocation cells as seen in Fig. 7. The presence of individual striation inside the dislocation cells can be observed more frequently. This dislocation striation penetrates the dislocation cells, leading to the formation of a smaller dislocation cell structure. The effects of the cyclic loading on the characteristics of dislocation structure are then investigated in the next section.

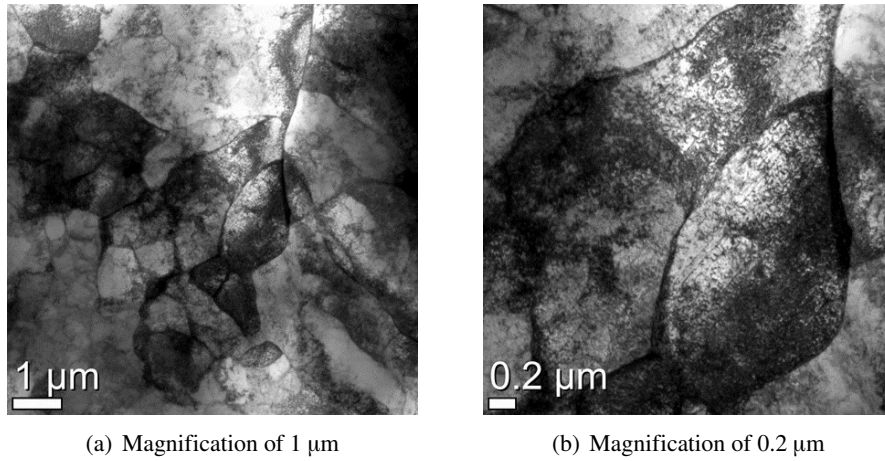


Figure 6. Dislocation structure of the specimens deformed by cyclic loading at $\varepsilon_a = 0.6\%$

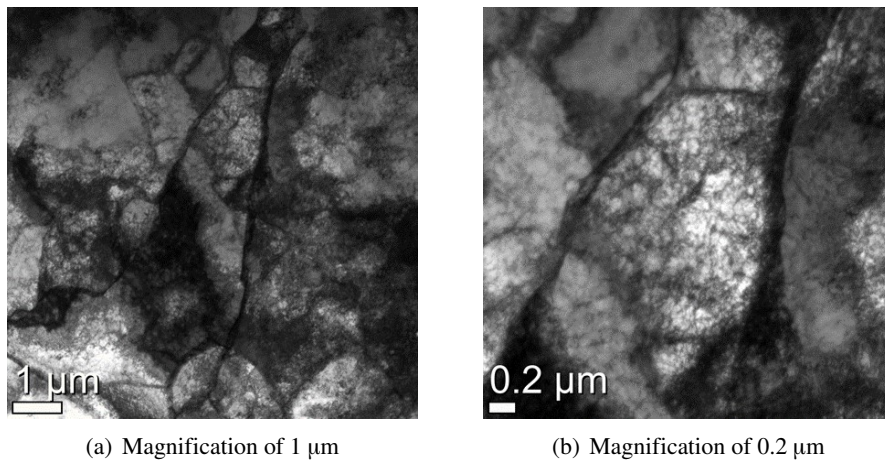
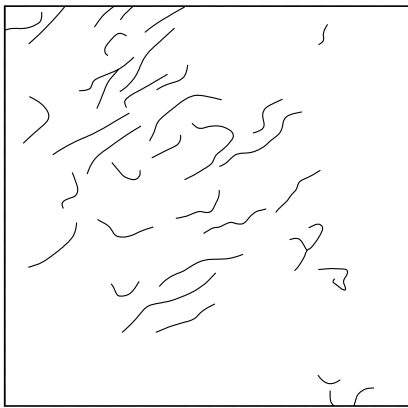


Figure 7. Dislocation structure of the specimens deformed by cyclic loading at $\varepsilon_a = 1.0\%$

4.2. Influences of low-cycle fatigue on the characteristics of dislocation structure

It has been known that dislocation density and dislocation cell size are two main characteristics of the dislocation structure. To characterize the influences of the cyclic loading on the characteristics of dislocation structure, the sketches of dislocation structures were conducted as shown in Fig. 8(a), Fig. 8(b), and Fig. 8(c) for corresponding the virgin sample and the samples deformed at strain amplitudes of 0.4% and 1.0%. Fig. 8(a) indicates that the dislocation density of the virgin specimen is quite low. By using the method presented in the previous section, the dislocation density can be determined using Eq. (6) based on the tested area and the number of intersections of the dislocation lines, and the surface plan. As a result, $\rho = 2.94 \times 10^{13} \text{ m}^{-2}$ was well calculated and reported for the virgin sample. It should be noted that the value of ρ was an average value calculated from three different tested areas. For the fatigue conditions, the same methodology was applied to determine the dislocation density, as a result, $\rho = 3.89 \times 10^{13} \text{ m}^{-2}$, $\rho = 4.36 \times 10^{13} \text{ m}^{-2}$, $\rho = 4.92 \times 10^{13} \text{ m}^{-2}$, and $\rho = 6.35 \times 10^{13} \text{ m}^{-2}$ were calculated for corresponding fatigue levels, i.e. strain amplitude of 0.4%, 0.6%, 0.8%, and 1.0%,

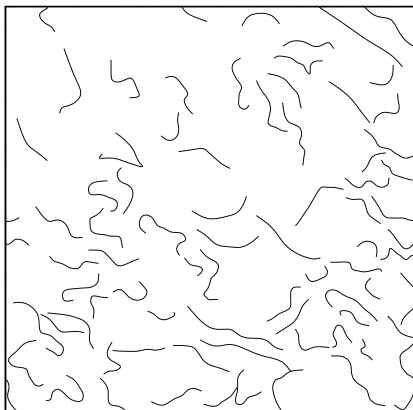
respectively. Consequently, the relationship between the dislocation density and strain amplitude was investigated and illustrated in Fig. 8. The results indicate that the applied strain amplitude strongly influences the dislocation density, in which the dislocation density tends to increase with the further increase of strain amplitude from 0.4% to 1.0%. This observation confirms the results of the evolution of dislocation structure in Figs. 4, 5, 6, and 7 as previously mentioned. Furthermore, it can be seen that this increase of dislocation density when the strain amplitude increases, seems to be linear. Indeed, the experimental data of dislocation density can be described as a linear function of the strain amplitude as, $\rho = 0.7856\epsilon_a + 2.1346$ with a good regression parameter ($R^2 = 0.9598$) as seen in Fig. 8.



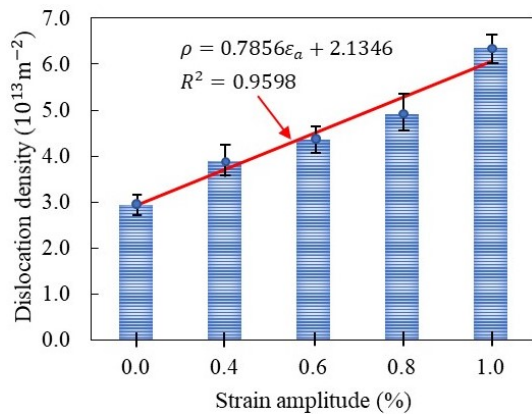
(a) Sketch of dislocation structure of the virgin specimen



(b) Sketch of dislocation structure of the specimen deformed at a strain amplitude of 0.4%



(c) Sketch of dislocation structure of the specimen deformed at a strain amplitude of 1.0%



(d) Influences of strain amplitude on dislocation density of deformed microstructure

Figure 8. Estimation of dislocation density and the effects of cyclic loading on dislocation density

Another characteristic of dislocation structure is the dislocation cell size. To investigate the influences of the fatigue condition on the dislocation cell size, the histogram showing the statistic of dislocation cell size distribution was conducted for strain amplitude levels. Based on the micro-images, the histogram for corresponding strain amplitude levels can be carefully constructed as illustrated in Fig. 9. It can be observed in Fig. 9(a) that the dislocation cell size varies in the wide range from 1000 nm

to 6000 nm, in which the dislocation cell size near 2000 nm is dominant, leading to an average dislocation cell size of 2690 ± 867 nm at a strain amplitude of 0.4%. When the fatigue condition increases, the dislocation cell size tends to decrease. Indeed, at a strain amplitude of 0.6%, the dislocation cell size varies from 800 nm to 4800 nm, in which the dislocation cell size close to 1200 nm is dominant, resulting in an average value of 2150 ± 739 nm. At the highest strain amplitude, an average value of 1570 ± 578 nm was well determined as shown in Fig. 9. Based on the calculation of dislocation cell size, the influence of fatigue condition on the mean dislocation cell size was well constructed as seen in Fig. 9(d). The results show that the dislocation cell size highly depends on the variation of strain amplitude levels, whereas the dislocation cell size tends to decrease characteristically with the further increase of fatigue conditions. This relationship can be described by a linear equation as $d = -1.88\varepsilon_a + 3.356$ with an R-square of 0.9558. This confirms the observation of dislocation structure as presented in Figs. 5, 6, and 7.

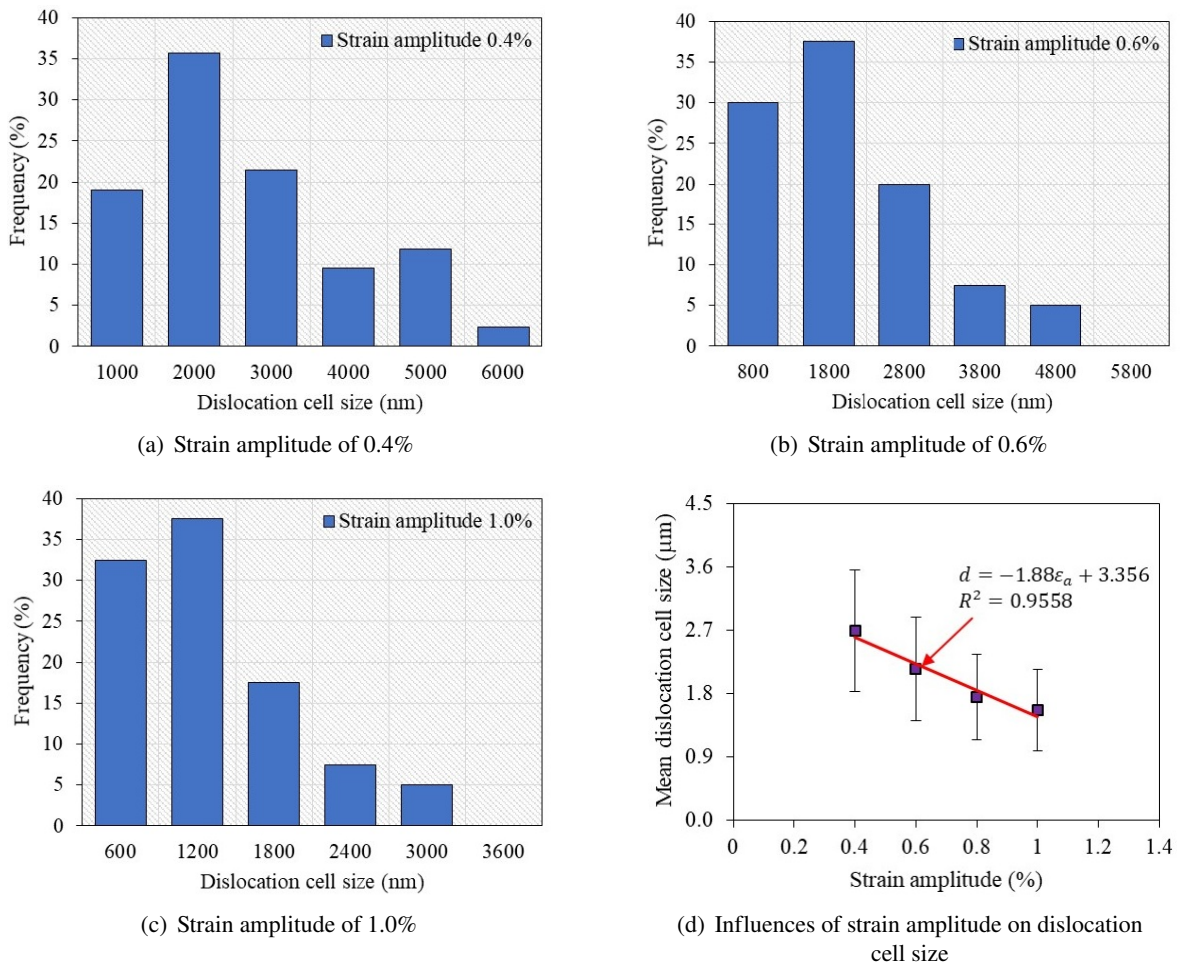


Figure 9. Variation of dislocation cell size under strain amplitude of low-cycle fatigue testing. Histogram showing the statistic of the dislocation cell size distribution

4.3. Relationship between the variation of dislocation structure and fatigue properties

The variation of microstructure under cyclic loading dominants the change in the mechanical properties of the specimens deformed by the low-cycle fatigue. By conducting the indentation experiments for four fatigue specimens, the variation of indentation hardness and yield stress of the material under cyclic loading can be investigated as seen in Fig. 10. It should be noted that indentation hardness can be determined using Eq. (1) based on the values of maximum applied load and the contact area, while the yield stress can be estimated using two dimensionless functions and the reverse algorithm. As seen in Fig. 10a, both indentation hardness and yield stress tend to increase with the further increase of strain amplitude level. Furthermore, these increases in mechanical properties seem to be linear. Based on the data of dislocation cell size and the variation of mechanical properties of the material, the relationship between the yield stress and dislocation cell size can be investigated and illustrated in Fig. 10(b). It can be seen that yield stress shows a decrease with the further increase of dislocation cell size. The relationship between the yield stress and dislocation cell size will be discussed later.

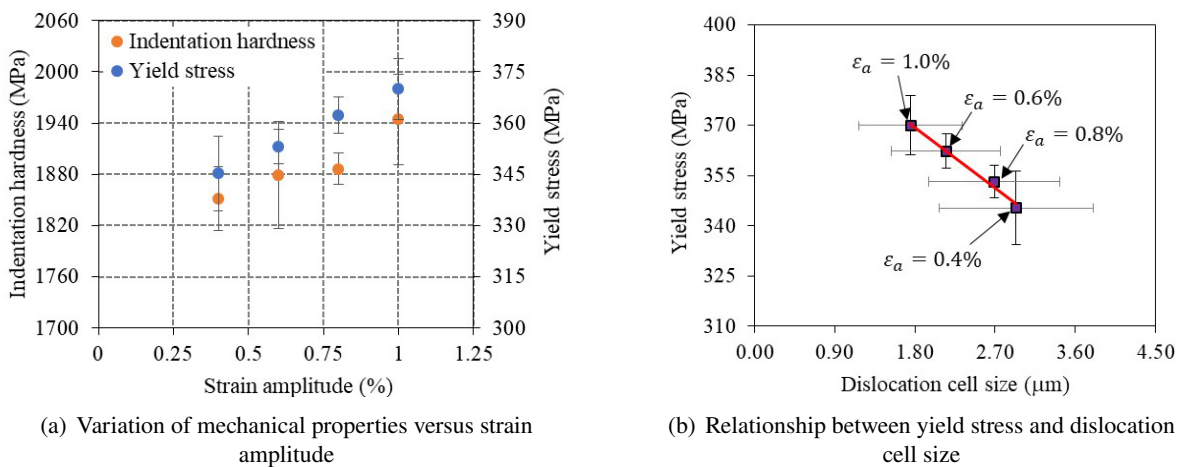


Figure 10. Effects of cyclic loading on mechanical properties and relationship between yield stress and dislocation cell size

The dislocation structure of the fatigue specimens was attributed to the main reason for the variation of mechanical properties with the further increase of strain amplitude from 0.4% to 1.0%. Indeed, when the applied stress range increases corresponding to the strain amplitude, the original grains are broken more as seen in Figs. 5, 6, and 7. This leads to the increase of dislocation density as seen in Fig. 8 as well as the degradation of dislocation cell size as illustrated in Fig. 9. The degradation of dislocation cell may result in the strengthening of fatigue mechanical properties as seen in Fig. 10. Hansen et al. [34] indicated that grain-boundary strengthening or Hall-Petch relation considered the grain boundaries act as pinning points impeding further dislocation propagation [35]. It means that there is an inverse relationship between delta yield strength and grain size. In other words, the relationship between yield stress and grain size can be described mathematically by the Hall–Petch equation as

$$\sigma_y = \sigma_0 + k_y / \sqrt{d} \quad (7)$$

where σ_y is the yield stress, σ_0 is a material constant for the starting stress for dislocation movement (or the resistance of the lattice to dislocation motion), k_y is the strengthening coefficient (a constant

specific to each material), and d is the average grain diameter. Additionally, Tabor [36] demonstrated that hardness is attributed as a function of yield stress through a material factor M , and thus the indentation hardness can also be described as a function of dislocation cell size as

$$H = M\sigma_y = M(\sigma_0 + k_y/\sqrt{d}) \quad (8)$$

It can be seen from Eqs. (7) and (8) that both indentation hardness and yield stress are inversely proportional to the value of dislocation cell size. Thus, it can be deduced from the characteristics of dislocation structure and the variation of fatigue properties that under cyclic loading, the dislocation cell structure was well-formed, and the dislocation density tended to increase, while the dislocation cell size tended to decrease with the further increase of fatigue conditions, resulting in the strengthening of yield stress.

5. Conclusions

In this study, the evolution of the dislocation cell structure and the variation of mechanical properties of structural steel subjected to cyclic loading was investigated using the depth-sensing indentation experiment and transmission electron microscope examinations. The experimental and analysis results support the following conclusions.

- Dislocation cell structure was well-formed under cyclic loading.
- Dislocation cell size tended to decrease from 2690 ± 867 nm to 1570 ± 578 nm, while dislocation density showed an increase from $3.89 \times 10^{13} \text{ m}^{-2}$ to $6.35 \times 10^{13} \text{ m}^{-2}$ with the further increase of strain amplitude from 0.4% to 1.0%, respectively.
- The relationship between dislocation density and fatigue condition can be described as $\rho = 0.7856\varepsilon_a + 2.135$.
- The relationship between dislocation cell size and strain amplitude can be described as $d = -1.88\varepsilon_a + 3.356$.
- Both indentation hardness and yield stress show an increase with the further increase of strain amplitude conditions.
- The change in the dislocation structure was responsible for the strengthening of fatigue properties, meaning that the dislocation density tended to increase, while the dislocation cell size showed a decrease with the further increase of fatigue condition, leading to the increase of both hardness and yield strength since mechanical properties were inversely proportional to the mean cell size.

Acknowledgments

This research was supported by a grant (19CTAP-C151846-01) from the Technology Advancement Research Program (TARP) funded by the Ministry of Land, Infrastructure, and Transport of the Korean government.

References

- [1] Luecke, W. E., McColskey, J. D., McCowan, C. N., Banovic, S. W., Fields, R. J., Foecke, T., Siewert, T. A., Gayle, F. W. (2005). Mechanical properties of structural steels. *National Institute of Standards and Technology, Washington*.
- [2] Pham, T.-H., Kim, S.-E. (2015). [Determination of mechanical properties in SM490 steel weld zone using nanoindentation and FE analysis](#). *Journal of Constructional Steel Research*, 114:314–324.

- [3] Pham, T.-H., Kim, S.-E. (2015). [Nanindentation for investigation of microstructural compositions in SM490 steel weld zone](#). *Journal of Constructional Steel Research*, 110:40–47.
- [4] Nguyen, N.-V., Kim, S.-E. (2020). [Experimental study to investigate microstructure and continuous strain rate sensitivity of structural steel weld zone using nanindentation](#). *International Journal of Mechanical Sciences*, 174:105482.
- [5] Nguyen, N.-V., Pham, T.-H., Kim, S.-E. (2019). [Strain rate sensitivity behavior of a structural steel during low-cycle fatigue investigated using indentation](#). *Materials Science and Engineering: A*, 744:490–499.
- [6] McCormac, J. C., Csernak, S. F. (2012). *Structural steel design*. Fifth edition, Pearson.
- [7] Boyer, H. E. (1987). *Atlas of Stress-Strain Curves*.
- [8] Soboyejo, W. (2002). *Mechanical properties of engineered materials*. CRC Press.
- [9] Ye, D., Xu, Y., Xiao, L., Cha, H. (2010). [Effects of low-cycle fatigue on static mechanical properties, microstructures and fracture behavior of 304 stainless steel](#). *Materials Science and Engineering: A*, 527 (16-17):4092–4102.
- [10] Ye, D., Mi, F., Liu, J., Xu, Y., Chen, Y., Xiao, L. (2013). [Use of instrumented indentation testing to study local mechanical properties of 304L SS welded joints subjected to low-cycle fatigue loadings](#). *Materials Science and Engineering: A*, 564:76–84.
- [11] Pham, T.-H., Kim, S.-E. (2016). [Microstructure evolution and mechanical properties changes in the weld zone of a structural steel during low-cycle fatigue studied using instrumented indentation testing](#). *International Journal of Mechanical Sciences*, 114:141–156.
- [12] Srinivasan, V. S., Sandhya, R., Bhanu, K., Rao, S., Mannan, S. L., Raghavan, K. S. (1991). [Effects of temperature on the low cycle fatigue behaviour of nitrogen alloyed type 316L stainless steel](#). *International Journal of Fatigue*, 13(6):471–478.
- [13] Ye, D., Matsuoka, S., Nagashima, N., Suzuki, N. (2005). [Multi-scale deformation behavior investigation of 18Cr–8Ni austenitic steel subjected to low-cycle fatigue loading](#). *Materials Characterization*, 55(2): 106–117.
- [14] Veerababu, J., Goyal, S., Sandhya, R., Laha, K. (2017). [Low cycle fatigue behaviour of Grade 92 steel weld joints](#). *International Journal of Fatigue*, 105:60–70.
- [15] Tsai, Y.-T., Lin, P.-C., Chen, Y.-W., Wang, S.-H., Yang, J.-R. (2018). [Fatigue behavior and microstructural characteristics of a duplex stainless steel weld metal under vibration-assisted welding](#). *Materials Science and Engineering: A*, 721:319–327.
- [16] Nguyen, N.-V., Pham, T.-H., Kim, S.-E. (2019). [Strain rate sensitivity behavior of a structural steel during low-cycle fatigue investigated using indentation](#). *Materials Science and Engineering: A*, 744:490–499.
- [17] Fukumoto, K., Onitsuka, T., Itoh, T., Sakasegawa, H., Tanigawa, H. (2018). [Microstructure of fatigue-tested F82H steel under multi-axial loadings](#). *Nuclear Materials and Energy*, 15:180–184.
- [18] Zhang, X., Wang, T., Gong, X., Li, Q., Liu, Y., Wang, Q., Zhang, H., Wang, Q. (2021). [Low cycle fatigue properties, damage mechanism, life prediction and microstructure of MarBN steel: Influence of temperature](#). *International Journal of Fatigue*, 144:106070.
- [19] Nguyen, N.-V., Pham, T.-H., Kim, S.-E. (2018). [Characterization of strain rate effects on the plastic properties of structural steel using nanindentation](#). *Construction and Building Materials*, 163:305–314.
- [20] Nguyen, N.-V., Kim, S.-E. (2020). [Experimental study to investigate microstructure and continuous strain rate sensitivity of structural steel weld zone using nanindentation](#). *International Journal of Mechanical Sciences*, 174:105482.
- [21] Hoan, P. T., Vinh, N. N., Tung, N. T. T. (2019). [Indentation for investigation of strain rate effect on mechanical properties in structural steel weld zone](#). *Journal of Science and Technology in Civil Engineering (STCE) - NUCE*, 13(3):104–112.
- [22] Oliver, W. C., Pharr, G. M. (1992). [An improved technique for determining hardness and elastic modulus using load and displacement sensing indentation experiments](#). *Journal of Materials Research*, 7(6):1564–1583.
- [23] Pham, T.-H., Kim, J. J., Kim, S.-E. (2015). [Estimating constitutive equation of structural steel using indentation](#). *International Journal of Mechanical Sciences*, 90:151–161.
- [24] Oliver, W. C., Pharr, G. M. (2004). [Measurement of hardness and elastic modulus by instrumented inden-](#)

- tation: Advances in understanding and refinements to methodology. *Journal of Materials Research*, 19 (1):3–20.
- [25] Cheng, Y.-T., Cheng, C.-M. (1998). [Scaling approach to conical indentation in elastic-plastic solids with work hardening](#). *Journal of Applied Physics*, 84(3):1284–1291.
- [26] Le, M.-Q. (2012). [Material characterization by instrumented spherical indentation](#). *Mechanics of Materials*, 46:42–56.
- [27] Pathak, S., Kalidindi, S. R. (2015). [Spherical nanoindentation stress–strain curves](#). *Materials Science and Engineering: R: Reports*, 91:1–36.
- [28] Dao, M., Chollacoop, N., Vliet, K. J. V., Venkatesh, T. A., Suresh, S. (2001). [Computational modeling of the forward and reverse problems in instrumented sharp indentation](#). *Acta Materialia*, 49(19):3899–3918.
- [29] Nguyen, N.-V., Kim, J. J., Kim, S.-E. (2019). [Methodology to extract constitutive equation at a strain rate level from indentation curves](#). *International Journal of Mechanical Sciences*, 152:363–377.
- [30] Pham, T.-H., Nguyen, N.-V. (2021). [Mechanical properties of constituent phases in structural steels and heat-affected zones investigated by statistical nanoindentation analysis](#). *Construction and Building Materials*, 268:121211.
- [31] ASTM-E3 (2011). *Standard Guide for Preparation of Metallographic Specimens*. ASTM Int. 1-12.
- [32] ISO 14577 (2002). *Metallic materials – Instrumented indentation test for hardness and materials parameters – Part 1: Test method*. Int. Organ. Stand. Geneva, Switz.
- [33] Oyen, M. (2010). *Handbook of Nanoindentation*. Pan Stanford Publishing.
- [34] Hansen, N. (2004). [Hall–Petch relation and boundary strengthening](#). *Scripta Materialia*, 51(8):801–806.
- [35] Wikipedia (2019). *Grain boundary strengthening*.
- [36] Tabor, D. (1951). *The hardness of metals*. Oxford University Press.